IOP Publishing Superconductor Science and Technology
Supercond. Sci. Technol. 31 (2018) 085001 (8pp) https://doi.org/10.1088/1361-6668/aac6a1

Superconductivity and phase diagram in a transition metal doped Zr_5Ge_3 compound

Sheng Li, Xiaoyuan Liu, Varun Anand and Bing Lv

Department of Physics, The University of Texas at Dallas, Richardson, TX 75080, United States of America

E-mail: blv@utdallas.edu

Received 19 March 2018, revised 11 May 2018
Accepted for publication 22 May 2018
Published 19 June 2018

Abstract

Systematic study of transition metal doped Zr_5Ge_3 at different sites has been performed, and superconductivity only occurs with Pt doping at the Ge site. Superconductivity remains absent with other transition metal doping such as Y, Cr, Ir, and Pd at other different sites. Coincidental with our previous findings in the $Zr_5Ge_{3-x}Ru_x$ system, it appears that the induced superconductivity is not only site-selective (only at the Ge site), but also dopant selective (only with Pt and Ru dopants). The bulk superconductivity in $Zr_5Ge_{3-x}Pt_x$ is investigated through magnetization, electrical resistivity, and heat capacity measurement, and the superconducting phase diagram of $Zr_5Ge_{3-x}Pt_x$ is also established.

Keywords: new superconductors, phase diagram, doping studies, Mn_5Si_3 structure type

(Some figures may appear in colour only in the online journal)

Introduction

Increasing research interest has emerged lately on the binary compound M_5X_3 (M = alkaline earth or transition metal, and X = main group elements including Al, Si and As families), which includes superconductivity [1–7], ferro/antiferromagnetism [8–12], host-interstitial chemistry [9–17], and high temperature structural applications [18–20]. These M_5X_3 phases are found crystallized in several different unique crystal systems, namely; hexagonal Mn_5Si_3-type [21], tetragonal Cr_5B_3 [22] and W_5Si_3-type [23], and orthorhombic Nb_5As_3 [24] and Y_5Bi_3-type [25] structures. Often, one compound might crystallize into two different structures, one as a high temperature phase and the other as a low temperature phase. For example, this is seen in both Ta_5Ge_3 [26] and Nb_5Si_3 [27] compounds. Chemical/interstitial doping [28, 29] was also found to be able to change the crystal structures upon doping, in turn, tuning the physical properties of the host binaries by the nature and amount of interstitial atoms that could be introduced.

Most of the Zr-based Zr_5X_3 (X = Sb, Pb, Sn, Ge, Si and Al) compounds are crystallized in the aforementioned Mn_5Si_3-type structure with space group $P6_3/mcm$ (#193). The essential feature of this structure is the presence of infinite $Zr_{6/2}X_3$ chains of confacial antiprisms of metal Zr on which the shared edges are bridged by isolated p-element atoms (anions) X, as shown in figure 1. The octahedral interstitial sites at the center of these confacial chains have been the subject of many studies, especially on the stabilization of pseudo-binary and ternary compounds with the Mn_5Si_3 structure. Superconductivity has been reported firstly in Zr_5Sb_3 with T_c ~2.3 K, and later in the Ru-doped Zr_5Sb_3 and Hf_5Sb_3 (with structure changing from Mn_5Si_3 type to W_5Si_3 type upon doping). Recently, we have successfully induced superconductivity in the Ru-doped Zr_5Ge_3 system, which remains the Mn_5Si_3 type structure upon chemical doping, with a possible unconventional superconductivity signature. Surprisingly, the superconductivity induction is doping-site-selective. With the same Ru doping, superconductivity only occurs with doping at the Ge site and remains absent with doping at the Zr site or an interstitial site above 1.8 K. This indicates some other competing factors, other than charge carrier changes caused by doping, may also play an important role. In this paper, we have taken an alternative approach to examining this issue, and carried out systematic doping studies at different sites for the Zr_5Ge_3 system. Chemical doping effects and structural instabilities caused by doping have been considered and tested for our doping studies in the Zr_5Ge_3 system. Surprisingly, superconductivity is only observed in the Pt doped $Zr_5Ge_{3-x}Pt_x$

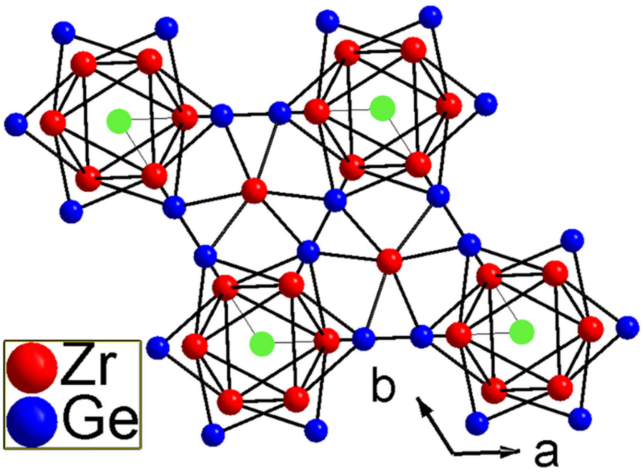

Figure 1. Projection of Zr_5Ge_3 structure along *c* directions. The small green circles at the corners of the unit cell show the octahedral interstitial 2b site formed by the trigonal antiprismatic Zr_6Ge_6 chain.

system besides our previous report on $Zr_5Ge_{3-x}Ru_x$ samples. We do not find superconductivity present in the same structure for Pd, or Ir doping studies in a similar manner above 1.8 K. Furthermore, no superconductivity is observed for chemical doping (both hole and electron) at the Zr site, nor at the structural instability boundaries upon chemical doping in Zr_5Ge_3 above 1.8 K. Our results suggest that Ge–Ru, and Ge–Pt are likely the critical charge-transfer pairs for the induced superconductivity, similar to the Sb–Ru pair reported in $Zr_5Sb_{3-x}Ru_x$ [2] and $Hf_5Sb_{3-x}Ru_x$ [30] compounds.

Experimental section

The polycrystalline samples were prepared through an arc melting technique on a water-cooled copper hearth in a home-made arc furnace under an argon-atmosphere, with Zr as a getter. All the Pt doped samples were synthesized under the same conditions. The starting materials are Zr pieces (99.8%, Strem Chemicals), Ge pieces (99.99%, Alfa Aesar), Pt pieces (99.9%, Alfa Aesar), Ir powder (99.95%), Y pieces (99.99%, Alfa Aesar), and Cr pieces (99.999%, Alfa Aesar). These starting materials were weighed in a glove box filled with argon gas. During the arc melting process, the melted samples were flipped and remelted several times to ensure homogeneity. The total weight loss of the samples was less than 1% before and after the arc melting process. After the arc melting process, the sample ingots are sealed into the Nb tubes first, and then subsequently sealed in an evacuated quartz tube which is then heated in the furnace at 1100 °C for one week for further annealing to ensure the sample homogeneity. The x-ray diffraction measurements were performed on the Rigaku Smartlab, and the Rietveld refinement of the XRD patterns was done through the JANA 2006 package. The dc magnetic moment $M(T, H)$ measurements were carried out using the MPMS (Quantum Design) down to 2 K. Resistivity and heat capacity as a function of temperature and field were measured with a PPMS-9T (Quantum Design) down to 1.8 K. Scanning electron microscopy (SEM) with energy dispersive x-ray analysis (EDX) is performed on a Zeiss-LEO 1530.

Results and discussions

The site-selective superconductivity induced in the Zr_5Ge_3 compound from the same amount of Ru doping has raised intriguing possibilities about the essentiality of the elements and the doping sites for the observed superconductivity in this system. One of the natural subsequent experiments to validate such assumptions will be to search for superconductivity in a similar system with the same structures. Our primary candidates will be similar noble metals such as Pd, Ir, and Pt, which have very similar chemical properties and doping effects as Ru metal.

As a matter of fact, Zr_5Ir_3 and Zr_5Pt_3 are known compounds that are crystallized in the same Mn_5Si_3-type structure, and this should facilitate the formation of a solid state solution in our doping studies and help to obtain uniform homogenous samples for the subsequent characterizations. As expected, the doping studies are quite successful. The x-ray powder pattern of several selected samples of different dopants and doping sites are presented in figure 2. Some small impurities are found in the Zr_5Ge_3 (as $ZrGe_2$ phase) and $Zr_5Ge_{2.5}Pd_{0.5}$ (as ZrPd phase) samples and all the others are XRD pure phase. The Rietveld refinements of the x-ray data indicate the high sample quality with good refinement value R_p and R_{wp}, and demonstrate that they all adopt the hexagonal Mn_5Si_3 type structure.

The temperature dependent electrical resistivity of several doped samples with the same doping level $x = 0.5$ of different $Zr_5Ge_{3-x}M_x$ (M = Pd, Ir, and Pt) and the parent compound Zr_5Ge_3 between 1.9 and 300 K are shown in figure 3(a). One can clearly see that superconductivity is only observed in the $Zr_5Ge_{2.5}Pt_{0.5}$ sample, and the other samples with the same doping level remain as poor metals in the measured temperature range above 1.9 K. The decreased residual-resistance ratio (RRR) in all the doped samples is expected from the enhanced scattering at low temperature caused by chemical doping. It is worthwhile to note that sometimes a small drop of resistivity is observed in the Ir-containing samples, which is attributed to small impurities of the superconducting Zr–Ir [31] alloy that is not detectable from XRD, but is evidenced from later SEM analysis. Apparently, the Pt element, similar to Ru, is critical for the induced superconductivity in the Zr_5Ge_3 system. Similarly, the induced superconductivity through Pt doping is also found to be site-selective. As shown in figure 3(b), with the same amount of Pt doping, only the Ge site doped sample $Zr_5Ge_{2.5}Pt_{0.5}$ is superconducting at 2.8 K, and the samples doped at the Zr site $Zr_{4.5}Pt_{0.5}Ge_3$ and at the octahedral interstitial site $Zr_5Ge_3Pt_{0.5}$ are found to be non-superconducting at our lowest measured temperature. These results further support our hypothesis that critical pairing of Ge–Ru and Ge–Pt is essential for the superconductivity in the Zr_5Ge_3 compound, similar to the observation found in the $Zr_5Sb_{3-x}Ru_x$ and $Hf_5Sb_{3-x}Ru_x$ compounds.

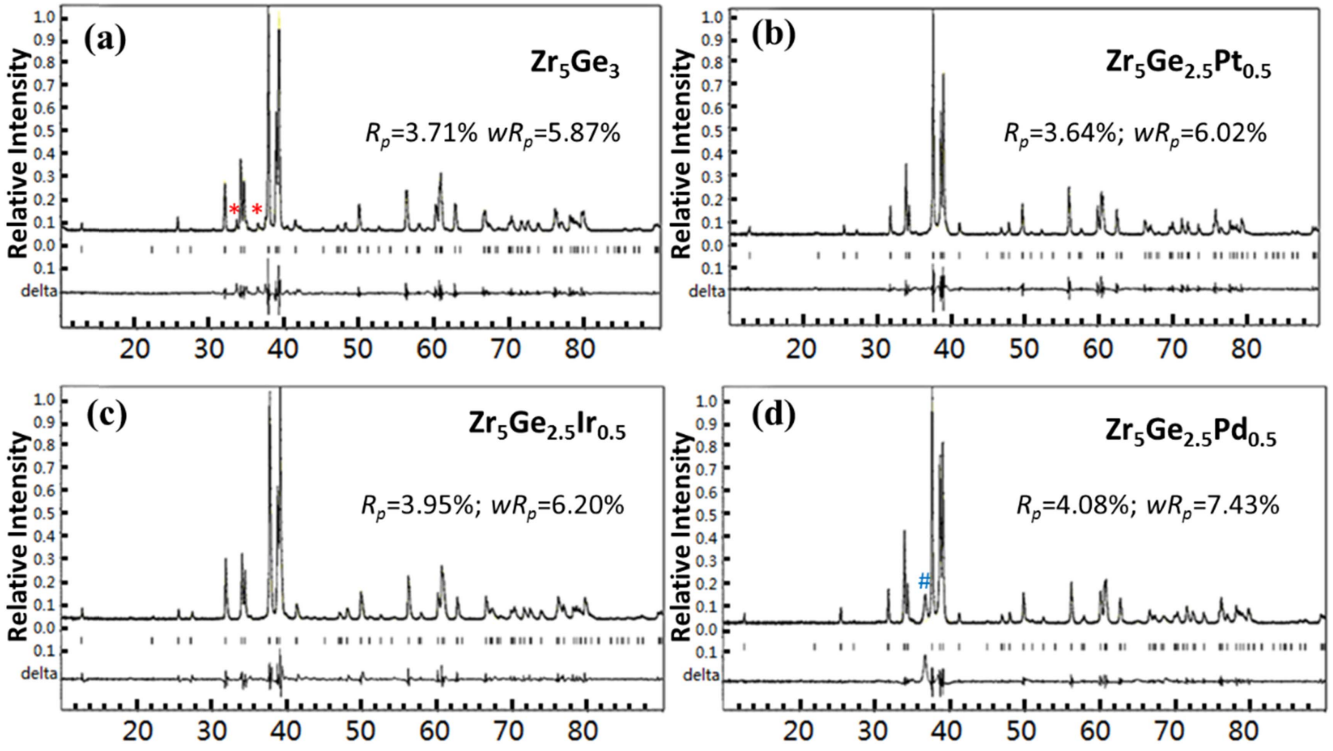

Figure 2. Rietveld refinement of the x-ray patterns for (a) Zr_5Ge_3, (b) $Zr_5Ge_{2.5}Pt_{0.5}$, (c) $Zr_5Ge_{2.5}Ir_{0.5}$, and (d) $Zr_5Ge_{2.5}Pd_{0.5}$ samples respectively. All the samples give good refinement value from the Rietveld refinement. The small impurity peaks are marked by* (as $ZrGe_2$) in Zr_5Ge_3 sample, and # (as ZrPd phase) for $Zr_5Ge_{2.5}Pd_{0.5}$ sample, respectively.

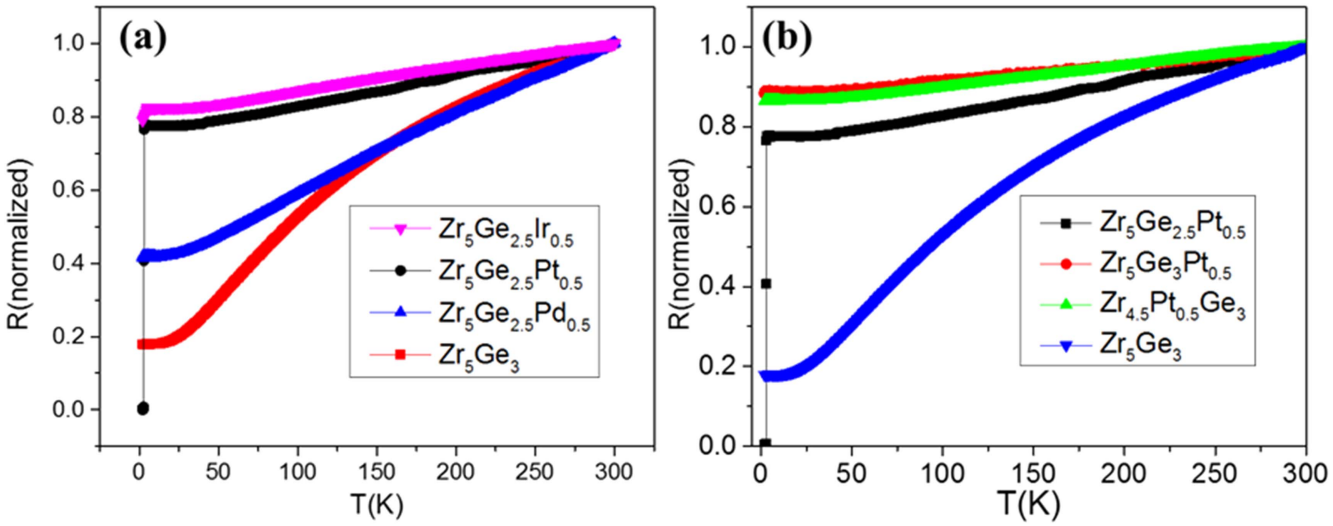

Figure 3. (a) Normalized temperature dependent resistivity data for different transition metal doped $Zr_5Ge_{3-x}M_x$ samples where only a Pt doped sample shows a superconducting behavior, (b) normalized temperature dependent resistivity data for different doped Zr_5Ge_3 samples with the same Pt amount but at a different site.

The fact that Zr_5Pt_3 crystallizes in the same Mn_5Si_3 type structure as Zr_5Ge_3 has allowed us to carry out systematic doping studies and explore the superconducting phase diagram of the $Zr_5Ge_{3-x}Pt_x$ system, in contrast to the $Zr_5Ge_{3-x}Ru_x$ system where observed phase separation prevents further studies of its doping dependence. We therefore have carried out several doping studies of $Zr_5Ge_{3-x}Pt_x$ samples with $x = 0$, 0.2, 0.5, 1.0 and 1.2, which are correspondent to doping levels of 0%, 6.7%, 16.7%, 33.3%, and 40%, respectively. A clear peak broadening is observed and some small impurities start to emerge at $x = 1$ for the Zr_5Ge_2Pt sample, indicating that phase separation starts occurring beyond this doping level. The formation of Zr_5Pt_3 phase occurs when $x > 1$. The Zr_5Pt_3 is known as a superconductor with T_c at 7.2 K, which essentially affects our analysis. Therefore, we only focus on the doped samples up to $x \leqslant 1$ for our following characterizations.

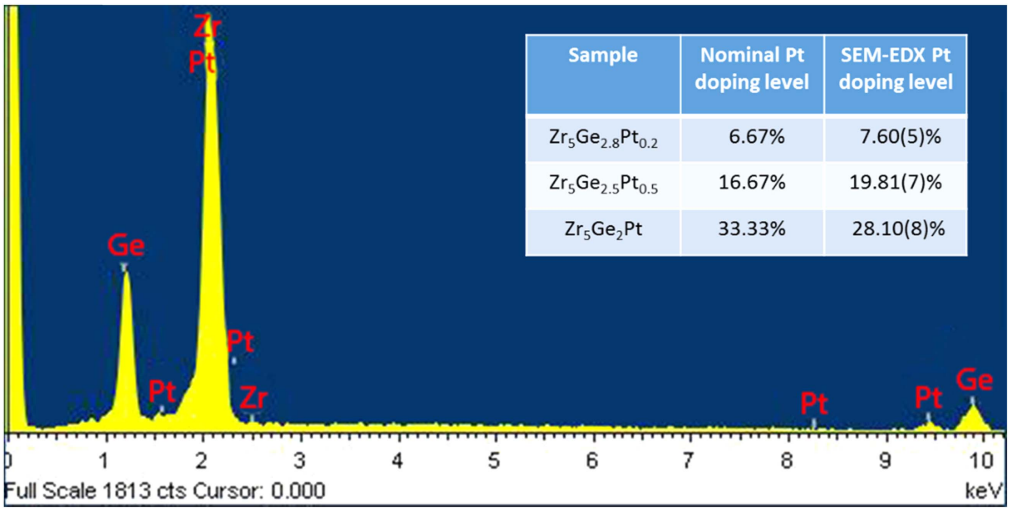

Sample	Nominal Pt doping level	SEM-EDX Pt doping level
$Zr_5Ge_{2.8}Pt_{0.2}$	6.67%	7.60(5)%
$Zr_5Ge_{2.5}Pt_{0.5}$	16.67%	19.81(7)%
Zr_5Ge_2Pt	33.33%	28.10(8)%

Figure 4. EDX analysis spectrum for one representative $Zr_5Ge_{3-x}Pt_x$ sample. The inset table shows the nominal element composition versus the actual composition from EDX analysis for samples with different Pt doping levels.

SEM-EDX analysis is performed for the Pt doped samples, and we found out that all three elements are uniformly distributed throughout the samples, and no other binary or elemental phases are observed. The representative SEM-EDX analysis spectrum is shown in figure 4, and the table of figure 4 shows the element ratio from EDX analysis, which is very close to our nominal composition for different doping levels, supporting the finding that chemical doping is successful and that the Pt indeed doped at the Ge site. The slightly larger discrepancy between the EDX result and the nominal composition for the higher doping level $x = 1$ sample indicates the beginning of the phase separation in this system, which is consistent with our previous XRD results.

The normalized resistivity data is shown in figure 5(a), with all the Pt doped samples showing a clear superconducting transition at low temperature, and the transition temperature of each sample increasing as the doping level increases from 2.6 K in $Zr_5Ge_{2.8}Pt_{0.2}$ to 3.5 K in Zr_5Ge_2Pt, shown in figure 5(b). The superconducting transition width is rather sharp, about 0.1 K for $Zr_5Ge_{2.8}Pt_{0.2}$ and $Zr_5Ge_{2.5}Pt_{0.5}$ samples. The slight broader transition (~0.5 K) in the Zr_5Ge_2Pt is likely due to the small impurities in the samples. Besides the superconducting transition, we can see a strong reduction of RRR as doping levels increased. The strong electron scattering in the Pt doped sample means there is a small free path of the electrons, which makes the system fall into the dirty limit so that the superconductivity of the $Zr_5Ge_{3-x}Pt_x$ material is not sensitive to the introduction of additional impurities and defects to the material.

The superconductivity in $Zr_5Ge_{3-x}Pt_x$ is further evidenced by the magnetic susceptibility $M(T)$ measurement. Figure 5(c) displays the $M(T, H)$ measured at 10 Oe for $Zr_5Ge_{2.5}Pt_{0.5}$ sample, both in the zero-field-cooled (ZFC) and field-cooled (FC) modes. A clear diamagnetic shift is observed below 2.8 K, shown in the figure 5(c). The shielding volume fraction derived from the ZFC curve is about 0.7 at 10 Oe at 2 K, and the ZFC curve does not become flat at our lowest measured temperature 2 K, indicating the actual superconducting volume could be even higher than 70%. This suggests that the superconductivity does originate from the bulk sample. The M–H loop at 1.8 K, shown in the figure 5(c) inset, shows the clear type-II superconductor characteristics, and the lower critical field H_{c1} is less than 20 Oe.

Based on the resistivity and magnetic data, we have proposed the phase diagrams of Pt doped $Zr_5Ge_{3-x}Pt_x$, presented in figure 5(d). One can see only a small doping level (~6.7%) is sufficient to induce superconductivity, and the superconducting T_c is monotonically increased with the doping level until a phase separation of Zr_5Pt_3 occurs when $x > 1$. It should be noted that superconductivity might be induced with an even lower doping level with a T_c below 2 K, which is beyond our lowest measurable temperature here. As Zr_5Pt_3 is also superconducting at a higher temperature with a T_c at 7.2 K, one may expect that the superconducting transition temperature will continue to increase if further doping studies are successful. The dashed line is the possible extrapolated doping dependence of T_c to the high levels until $x = 3$, if no phase separation occurs.

As the Zr_5Ge_2Pt sample is not quite ideal (slightly broadened superconducting transition due to impurities, as discussed before), we have used the $Zr_5Ge_{2.5}Pt_{0.5}$ sample to determine the precise upper critical field through magnetoresistance $\rho(T, H)$ measurements. The magnetoresistivity data is shown in figure 6(a). One can see that with the highest applied 1 T magnetic field, the transition temperature decreases less than 0.5 K, which indicates high upper critical field in this system. Taking the 10% resistivity drop as a criterion, we can extrapolate the H_{c2} value to zero temperature using the Werthamer–Helfand–Hohenberg (WHH) theory. The calculated upper critical field is 4.3 T through the WHH fitting, shown as the inset in figure 5(b). The upper critical field is comparable to the superconducting Zr_5Sb_3 sample with the same crystal structure, which has superconducting T_c at 2.3 K and upper critical field H_{c2} at 3.4 T.

The bulk superconductivity in $Zr_5Ge_{2.5}Pt_{0.5}$ can be further demonstrated by the pronounced specific heat anomaly in

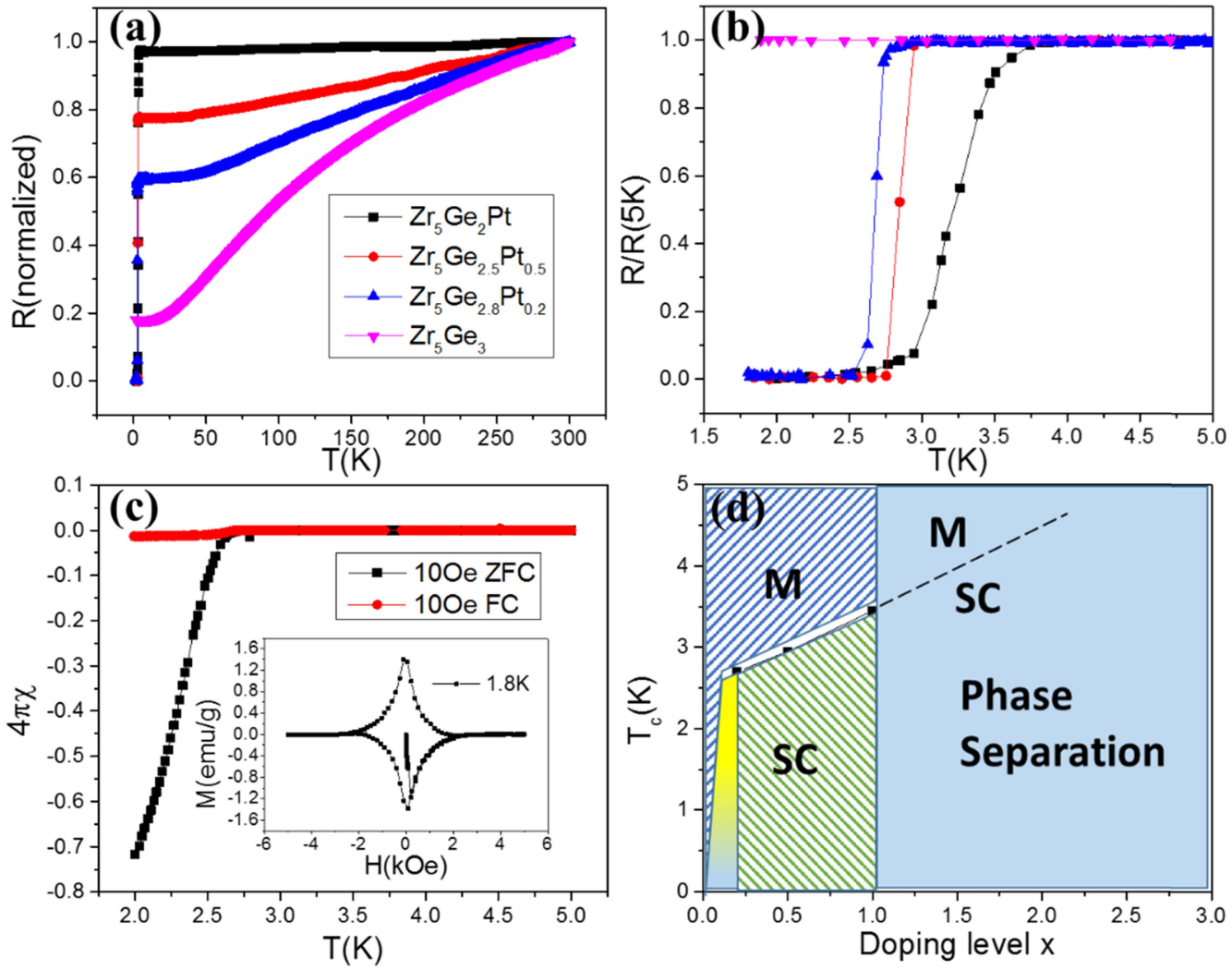

Figure 5. (a) Normalized temperature dependent resistivity data for Pt doped $Zr_5Ge_{3-x}Pt_x$ samples with different doping level ($x = 0$, 0.2, 0.5 and 1.0); (b) the superconducting transition for different samples on an enlarged scale between 1 and 5 K; (c) magnetization measurement data in ZFC and FC modes at 10 Oe for the $Zr_5Ge_{2.5}Pt_{0.5}$ sample, the inset shows the *M–H* loop at 1.8 K, (d) superconducting phase diagram of $Zr_5Ge_{3-x}Pt_x$. The superconductivity might already be induced in the gradient yellow area ($x < 0.2$), with T_c below 2 K which is below our lowest measureable temperature.

figure 7. By subtracting the normal state specific data, we can determine the electronic contributions in the superconducting state. A superconducting specific heat anomaly appears at 2.5 K, with the specific heat jump of about $\Delta C/T_c \sim 12\,\mathrm{mJ\,mol^{-1}\,K^{-2}}$ at a zero magnetic field. From the Debye fitting of normal specific heat data at 5 T using $C = \gamma_n T + \beta T^3$, we can get $\gamma_n = 16.15\,\mathrm{mJ\,mol^{-1}\,K^{-2}}$, and $\beta = 0.48\,\mathrm{mJ\,mol^{-1}\,K^{-4}}$, which corresponds to the electronic Sommerfeld coefficient and Debye temperature respectively. The Debye temperature can be deduced from the β value through the relationship $\Theta_D = (12\pi^4 k_B N_A Z/5)^{1/3}$, where $N_A = 6.02 \times 10^{23}\,\mathrm{mol^{-1}}$ as the Avogadro constant, and Z is the number of atoms in the molecule. The obtained Debye temperature is about 325 K. From γ_n and $\Delta C/T_c$ we get the $\Delta C/\gamma_n T_c$ about 0.72, which is much smaller than the BCS value 1.43.

As our lowest measured temperature of 1.8 K is only slightly lower than the superconducting transition (~2.8 K), we could not have the overall picture of the exponential decay of $Ce/T(T)$ below T_c and perform meaningful fitting to the extended α-model. However, this small value of $\Delta C/\gamma_n T_c$ reveals that the $Zr_5Ge_{2.5}Pt_{0.5}$ is a superconductor with a rather weak electron–phonon coupling, which is consistent with our previous observation in the $Zr_5Ge_{2.5}Ru_{0.5}$ system. The Sommerfeld coefficient is found to be $12.85\,\mathrm{mJ\,mol^{-1}\,K^{-2}}$ for parent Zr_5Ge_3 compound. As the Sommerfeld coefficient is proportional to the density of states (DOS) at the Fermi level, the 25% enhancement of γ_n from $12.85\,\mathrm{mJ\,mol^{-1}\,K^{-2}}$ in Zr_5Ge_3 to $16.15\,\mathrm{mJ\,mol^{-1}\,K^{-2}}$ in $Zr_5Ge_{2.5}Pt_{0.5}$ upon Pt doping implies the enhancement of the DOS which may take responsibility for the observed superconductivity in Pt doped Zr_5Ge_3 samples. Please note that the residual carrier contribution γ_0 obtained from linear fitting of the 0 T data is $6.55\,\mathrm{mJ\,mol^{-1}\,K^{-2}}$, and this value might be slightly overestimated due to few data being used for liner extrapolation below the superconducting transition. Therefore, the superconducting volume fraction estimated from heat capacity analysis, $(\gamma_n - \gamma_0)/\gamma_n \sim 60\%$, as the lower limit of

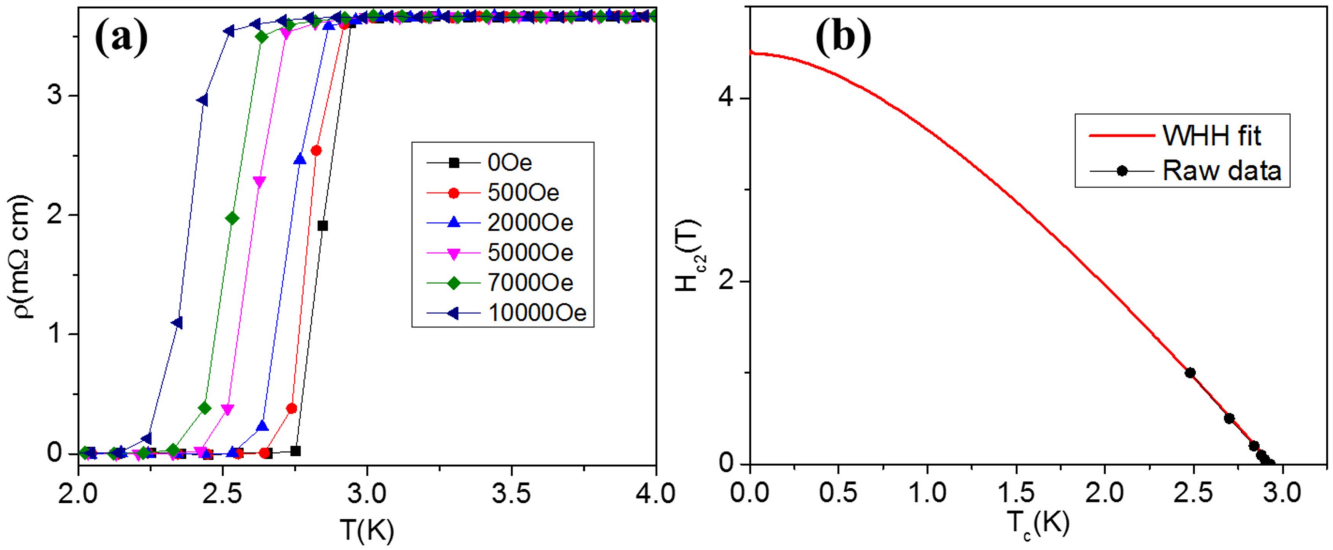

Figure 6. (a) Field dependence resistivity data at low temperature for $Zr_5Ge_{2.5}Pt_{0.5}$ sample, and (b) the upper critical field H_{c2} (T) and its fitting by the WHH theory.

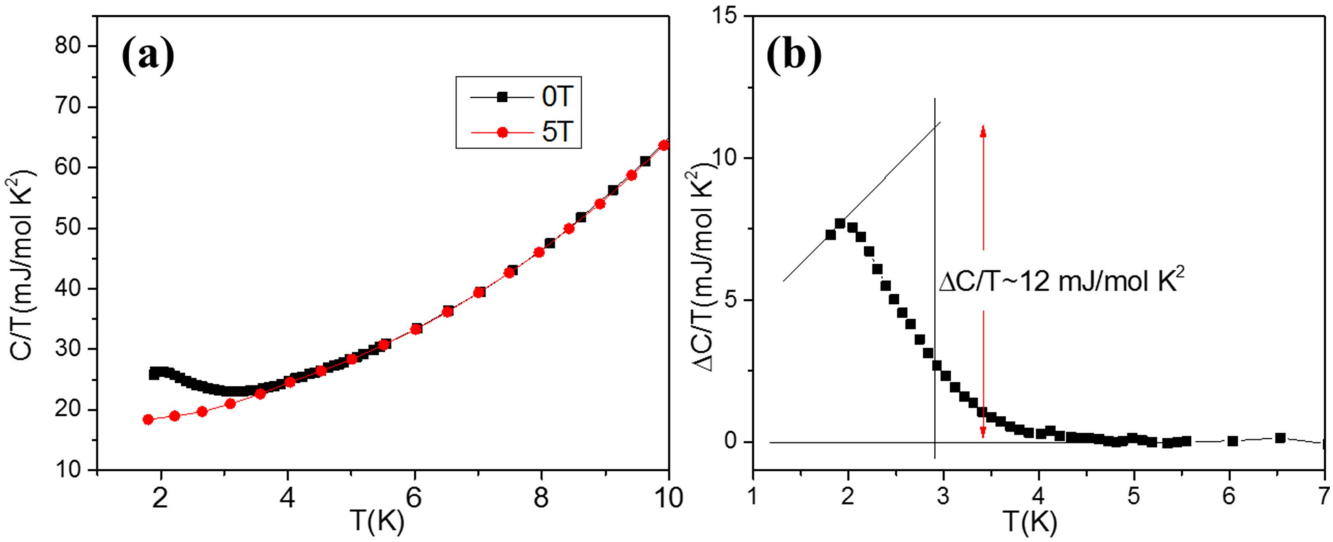

Figure 7. (a) Heat capacity data of $Zr_5Ge_{2.5}Pt_{0.5}$ sample at different magnetic field where a clear specific heat jump is visible below 3 K at zero-field; (b) the difference of electronic specific heat data between the normal state and superconducting state of $Zr_5Ge_{2.5}Pt_{0.5}$ sample.

superconducting volume fraction, indeed suggests the bulk superconducting in this compound, and is consistent with our magnetic results.

To further test our hypothesis that critical pairing of the Ge–Ru and Ge–Pt is essential for the superconductivity in the Zr_5Ge_3 system, we carried out additional doping studies with both hole doping with Y and electron doping with Cr at the Zr site. As the Y_5Ge_3 compound also adopts the same Mn_5Si_3 type structure, it should also be rather easy to form a solid solution for the doping studies. But for the Cr doping, the Cr_5Ge_3 is crystallized in the tetragonal W_5Si_3 structure, therefore one would expect structural transformation from the Mn_5Si_3 type to the W_5Si_3 type structure at certain doping levels if the doping studies are successful. The XRD patterns of $Zr_{5-x}Y_xGe_3$ ($x = 1$) and $Zr_{5-x}Cr_xGe_3$ ($x = 1$), together with the parent compound Zr_5Ge_3, are presented in figure 8(a). It is clear that the Y-doped sample is of good quality with the same Mn_5Si_3 type structure, although a slight peak broadening is observed. But for the Cr doped sample, impurity peaks that belong to the $ZrCrGe_2$ [32] phase emerge, although the major phase (>80%) is still crystallized in the hexagonal Mn_5Si_3-type structure. The nominal doping level of both Y and Cr is 20%, which is close to the doping level of $Zr_5Ge_{2.5}Pt_{0.5}$ (~16.7%). Such a high doping level, which may significantly enhance the carrier concentrations, typically should be sufficient to induce superconductivity in the Zr_5Ge_3 if successful. From the normalized temperature dependent resistivity data in figure 8(b), both samples show a clear increase of the RRR value with Y and Cr doping, as expected. However, we do not observe any superconductivity signature in both electron and hole doped samples above 1.8 K. This further supports our conjecture that both the doping-site and

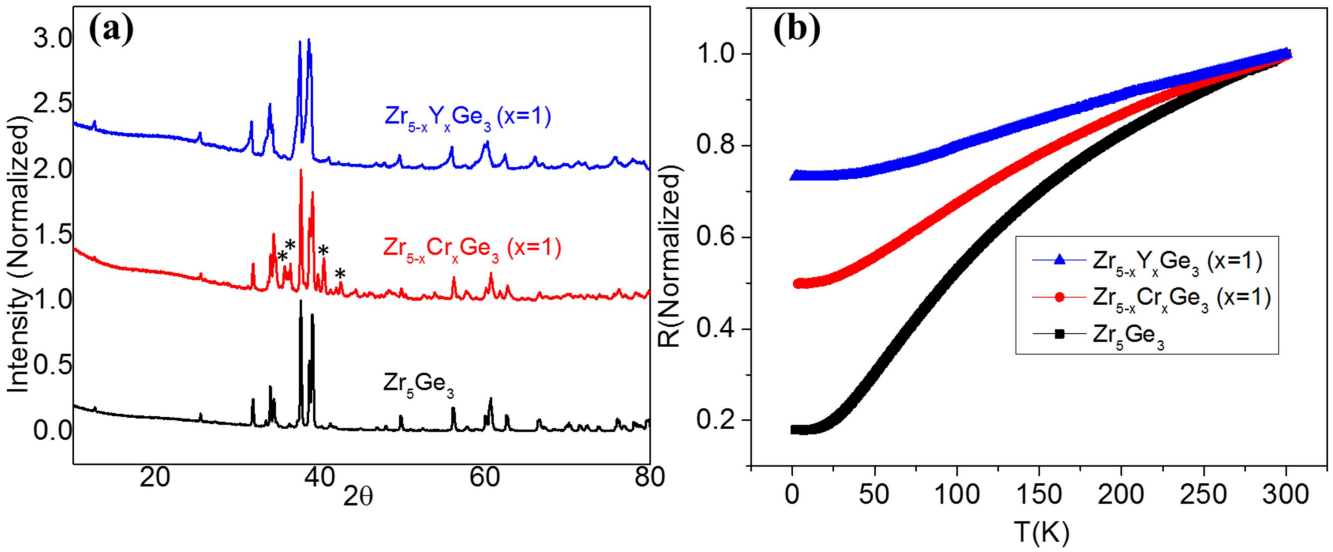

Figure 8. (a) XRD patterns for Zr_5Ge_3, $Zr_{5-x}Y_xGe_3(x = 1)$, and $Zr_{5-x}Cr_xGe_3(x = 1)$ doped samples. The impurity peaks of $ZrCrGe_2$ are marked as * in the Cr doped sample. (b) Normalized temperature dependent resistivity data of Zr_5Ge_3, and both electron (Cr) and hole (Y) doped samples.

dopant are very selective for inducing superconductivity in the Zr_5Ge_3 system.

Summary

In summary, we have systematically investigated the doping studies of Zr_5Ge_3 with different transition metals and found out that only Pt and Ru doping are able to induce superconductivity in the Zr_5Ge_3 compound. The superconductivity is found to be not only site-selective (only at the Ge site), but also dopant selective (only with Ru or Pt dopants). The Ge–Ru and Ge–Pt are essentially some critical-pair elements for the superconductivity in the Zr_5Ge_3 compound, similar to the observation found in the $Zr_5Sb_{3-x}Ru_x$ and $Hf_5Sb_{3-x}Ru_x$ compounds. The bulk superconductivity in the $Zr_5Ge_{3-x}Pt_x$ is investigated through magnetization, electrical resistivity, and heat capacity measurement, and a superconducting phase diagram is established. Further heat capacity analysis suggests rather weak electron–phonon coupling in the superconducting compound, and that the enhancement of DOS at the Fermi level through Pt doping might be responsible for the induced superconductivity.

Acknowledgments

The authors would like to acknowledge the US Air Force Office of Scientific Research (AFOSR), and the Start-Up funds from University of Texas at Dallas for financial support.

ORCID iDs

Bing Lv https://orcid.org/0000-0002-9491-5177

References

[1] Lv B, Zhu X Y, Lorenz B, Wei F Y, Xue Y Y, Yin Z P, Kotliar G and Chu C W 2013 *Phys. Rev.* B **88** 134520
[2] Xie W W, Luo H X, Phelan B F and Cava R J 2015 *J. Mater. Chem.* C **3** 8235–40
[3] Li S, Liu X, Anand V and Lv B 2018 *New J. Phys.* **20** 013009
[4] McGuire M A and Parker D S 2016 *Phys. Rev.* B **93** 064507
[5] Corrêa L E, da Luz M S, de Lima B S, Cigarroa O V, da Silva A A A P, Coelho G C, Fisk Z and Machado A J S 2016 *J. Alloys Compd.* **660** 44–7
[6] Kawashima K, Muranaka T, Kousaka Y, Akutagawa S and Akimitsu J 2009 *J. Phys.: Conf. Ser.* **150** 052106
[7] Waterstrat R M, Kuentzler R and Muller J 1990 *J. Less-Common. Met.* **167** 169–78
[8] Brown P J and Forsyth J B 1995 *J. Phys.: Condens. Matter* **7** 7619
[9] Zeng C G, Erwin S C, Feldman L C, Li A P, Jin R, Song Y, Thompson J R and Weitering H H 2003 *Appl. Phys. Lett.* **83** 5002
[10] McGuire M A and Parker D S 2015 *J. Appl. Phys.* **118** 163903
[11] Tkachuk A, Gorelenko Y, Padlyak B, Jankowska-Frydel A and Stadnyk Y 2002 *J. Magn. Magn. Mater.* **242–245** 901–3
[12] Drzyzga M and Szade J 2001 *J. Alloys Compd.* **321** 27–34
[13] Garcia E and Corbett J D 1990 *Inorg. Chem.* **29** 3274–82
[14] Corbett J D, Garcia E, Guloy A M, Hurng W, Kwon Y and Alejandro Leon-Escamilla E 1998 *Chem. Mater.* **10** 2824–36
[15] Kim S J, Kematick R J, Yi S S and Franzen H F 1988 *J. Less-Common. Met.* **137** 55–9
[16] Kwon Y, Rzeznik M A, Guloy A and Corbett J D 1990 *Chem. Mater.* **2** 546–50
[17] Wu H, Zhou W, Udovic T J, Rush J J and Yildirim T 2008 *Chem. Phys. Lett.* **460** 432–7
[18] Leon-Escamilla E A and Corbett J D 2001 *J. Solid State Chem.* **159** 149–62
[19] Zhao M, Nakayama S, Hatakeyama T, Nakamura J and Yoshimi K 2017 *Intermetallics* **90** 169–79
[20] Ito K, Ihara K, Tanaka K, Fujikura M and Yamaguchi M 2001 *Intermetallics* **9** 591–602
[21] Lander G H, Brown P J and Forsyth J B 1967 *Proc. Phys. Soc.* **91** 332

[22] Bertaut F and Blum P 1953 *C. R. Hebd. Seances Acad. Sci.* **236** 1055–6
[23] Aronsson B 1955 *Acta Chem. Scand.* **9** 1107–10
[24] Laohavanich S, Thanomkul S and Pramatus S 1982 *Acta Cryst.* B **38** 1398
[25] Wang B C, Gabe E J, Calvert L D and Taylor J B 1976 *Acta Cryst.* B **32** 1440–5
[26] Yuan F, Forbes S, Ramachandran K K and Mozharivskyj Y 2015 *J. Alloys Compd.* **650** 712–7
[27] Massalski T B 1990 *Binary Alloy Phase Diagrams* vol 175 2nd edn (Materials Park, OH: ASM International) p 730
Knapton A G 1955 *Nature* **175** 730
[28] Bortolozo A D, dos Santos C A M, Jardim R F, Ritter C, Devishvili A, Rotter M, Gandra F G and Machado A J S 2012 *J. Appl. Phys.* **111** 123912
[29] Leon-Escamilla E A and John D C 2001 *Inorg. Chem.* **40** 1226–33
[30] Xie W W, Luo H X, Seibel E M, Nielsen M B and Cava R J 2015 *Chem. Mater.* **27** 4511–4
[31] Matthias B T, Corenzwit E and Compton V B 1961 *J. Phys. Chem. Solids* **19** 130
[32] Yamolyuk Y P, Sikiritsa M, Aksel'rud L G, Lysenko L A and Gladyshevskii E I 1982 *Sov. Phys.—Crystallogr.* **27** 652–3